Optimized Synthesis of the Elusive ϵ-Fe_2O_3 Phase via Sol−Gel Chemistry

Mihaela Popovici,[†] Martí Gich,*[,‡] Daniel Nižňanský,[§] Anna Roig,[‡] Cecilia Savii,[†] Lluís Casas,[‡] Elies Molins,[‡] Karel Zaveta,[||] Corina Enache,[†] Jordi Sort,[⊥] Sophie de Brion,[#] Gerard Chouteau,[#] and Josep Nogués[+]

Institute of Chemistry Timisoara of Romanian Academy, 24 Mihai Viteazul Blvd., RO-300223 Timisoara, Romania, Institut de Ciència de Materials de Barcelona (ICMAB-CSIC), Esfera UAB, 08193 Bellaterra, Catalunya, Spain, Institute of Inorganic Chemistry, Academy of Sciences of Czech Republic, 250 68, Řež near Prague, Czech Republic, Joint Laboratory for Mössbauer Spectroscopy, Faculty of Mathematics and Physics, Charles University, V Holesovickach 2, 180 00 Prague 8, Czech Republic, SPINTEC (URA 2512 CNRS/CEA), CEA/Grenoble, 17 Av. Martyrs, 38054 Grenoble Cedex 9, France, Grenoble High Magnetic Field Laboratory, CNRS B.P. 166, Grenoble 38042 Cedex 9, France, and Institució Catalana de Recerca i Estudis Avançats (ICREA) and Departament de Física, Universitat Autònoma de Barcelona, 08193 Bellaterra, Catalunya, Spain

Received August 17, 2004

ϵ-Fe_2O_3 nanoparticles embedded in a SiO_2 matrix have been synthesized by sol−gel chemistry and high temperature heat treatments. Virtually pure ϵ-Fe_2O_3 (in excess of 93%) is obtained, although a two-phase mixture, ϵ-Fe_2O_3 + α-Fe_2O_3, is observed for Fe_2O_3/SiO_2 ratios greater than 37 wt %. The ϵ-Fe_2O_3 nanoparticles are stable up to ~1600 K. Optimized ϵ-Fe_2O_3 nanoparticles are ferrimagnetic, with a Curie temperature $T_C \approx 510$ K, and remarkably high values of room-temperature coercivity, $H_C = 20$ kOe.

1. Introduction

Iron(III) oxides are among the most common iron compounds found in nature, and they are readily synthesized. Hematite, α-Fe_2O_3, is the most stable of the iron oxides in ambient conditions. However, there are a number of polymorphs of the iron(III) oxide system: α-Fe_2O_3 (hematite); γ-Fe_2O_3 (maghemite); ϵ-Fe_2O_3; β-Fe_2O_3; and amorphous Fe_2O_3.[1,2] Because of its technological applications in magnetic recording, γ-Fe_2O_3 is perhaps the most extensively studied polymorph,[3] and ϵ-Fe_2O_3 is a rare polymorph that is difficult to synthesize as a single-phase sample. This phase is particularly interesting because, in fine particle form, it exhibits very large coercive field values.[4] Natural occurrences of ϵ-Fe_2O_3 have been reported in some plants, as biogenic nanoparticles[5] and as thermal decomposition products of almandine garnets[6,7] and iron-rich clays.[8] A number of different techniques have been proposed to synthesize ϵ-Fe_2O_3. Pioneering works were based on thermal decompositions in air of Fe precursors,[9] or on the oxidation of Fe-containing species promoted by fast energy deposition techniques. In the thermal decomposition experiments, Fe_2O_3 mixed oxides,[9] basic ferric salts,[10,11] and other precipitates,[12] obtained from ferric iron salts in basic solutions, were thermally treated. Concerning high-energy deposition syntheses, techniques such as electric discharge,[13] gamma irradiation,[14] or laser-assisted pyrolysis[15] were used to oxidize vaporized Fe, Fe(II) formate, and an $Fe(CO)_5-N_2O$ gas mixture, respectively. More recently, the sol−gel approach has opened new scenarios for the synthesis of the ϵ-Fe_2O_3 polymorph.[16−18] Silicon alkox-

* Corresponding author. E-mail: mgich@icmab.es.
[†] Institute of Chemistry Timisoara of Romanian Academy.
[‡] Institut de Ciència de Materials de Barcelona, Esfera UAB.
[§] Academy of Sciences of Czech Republic.
[||] Charles University.
[⊥] SPINTEC.
[#] Grenoble High Magnetic Field Laboratory, CNRS.
[+] Institució Catalana de Recerca i Estudis Avançats (ICREA) and Departament de Física, Universitat Autònoma de Barcelona.

(1) Cornel, R. M.; Schwertmann, U. *The Iron Oxides. Structure, Properties, Reactions Occurrence and Uses*; VCH: Weinheim, 1996.
(2) Zboril, R.; Mashlan, M.; Petridis, D. *Chem. Mater.* **2002**, *14*, 969.
(3) Dorman, J. L.; Fiorani, D.; Tronc, E. *Adv. Phys. Chem.* **1997**, *98*, 283.
(4) Jin, J.; Ohkoshi, S.; Hashimoto, K. *Adv. Mater.* **2004**, *16*, 48.
(5) McClean, R. G.; Schofield, M. A.; Kean, W. F.; Sommer, C. V.; Robertson, D. P.; Toth, D.; Gajdardziska-Josifovska, M. *Eur. J. Mineral.* **2001**, *13*, 1235.
(6) Barcova, K.; Mashlan, M.; Zboril, R.; Martinec, P.; Kula, P. *Czech. J. Phys.* **2001**, *51*, 749.
(7) Barcova, K.; Mashlan, M.; Martinec, P. *Hyperfine Interact.* **2002**, *139*, 463.
(8) Van Wonterghem, J.; Mørup, S.; Villadsen, J.; Koch, C. J. H. *J. Mater. Sci.* **1987**, *22*, 438.
(9) Forrestier, H.; Guiot-Guillain, G. C. *C. R. Acad. Sci. (Paris)* **1934**, *199*, 720.
(10) Walter-Levy, L.; Quemeneur, M. E. *C. R. Acad. Sci. (Paris)* **1963**, 257, 3410.
(11) Kato, A.; Matuya, S. *Denki Kagaku* **1977**, *45*, 285.
(12) Trautmann, J.-M.; Forestier, H. *C. R. Acad. Sci. (Paris)* **1965**, *261*, 4423.
(13) Schrader, R.; Buttner, G. *Z. Anorg. Allg. Chem.* **1963**, *320*, 220.
(14) Doroshenko V. N.; Kaurkovskaya, V. N.; Yakubenko, E. P.; Pobokin, D. I.; Entinzon, I. R.; Ogenko, V. M. *High Energy Chem.* **2002**, *36*, 157.
(15) Martelli, S.; Mancini, A.; Giorgi, R.; Alexandrescu, R.; Cojocaru, S.; Crunteanu, A.; Voicu, I.; Balu, M.; Morjan, I. *Appl. Surf. Sci.* **2000**, *154−155*, 353.
(16) Viart, N. Thesis, University Strasbourg, 1996.
(17) Chanéac, C.; Tronc E.; Jolivet, J. P. *Nanostruct. Mater.* **1995**, *6*, 715.
(18) Dormann, J. L.; Viart N.; Rehspringer, J. L.; Ezzir, A.; Niznansky, D. *Hyperfine Interact.* **1998**, *112*, 89.

10.1021/cm048628m CCC: $27.50
Published on Web 11/17/2004

ides with Fe nitrate precursors are an effective way to synthesize ϵ-Fe_2O_3, but typically they yield mixtures of ϵ-Fe_2O_3 plus α-Fe_2O_3 and/or γ-Fe_2O_3. Although some of the classical works in ϵ-Fe_2O_3 reported single-phase material,[9,12,19] subsequent studies indicated that yields of greater than 70% ϵ-Fe_2O_3 are difficult to obtain.[2] Nevertheless, it has been recently reported that the addition of Ba^{2+} or Sr^{2+} ions in the synthesis appears to stabilize the ϵ-Fe_2O_3 phase.[4] The formation of ϵ-Fe_2O_3 is very sensitive to synthesis conditions, for example, oxidizing power of the atmosphere (oxygen, air), duration of the oxidation, or the presence of hydroxyl groups (excess water, high hydrolysis ratio). Interestingly, most studies cited herein seem to indicate that ϵ-Fe_2O_3 can only be synthesized in nanoparticle form, which suggests that surface effects may play an important role in the formation of this phase.

Reported properties of ϵ-Fe_2O_3 are controversial, in part, because it is difficult to synthesize pure ϵ-Fe_2O_3. For example, the crystal structure of ϵ-Fe_2O_3 has been reported as deformed rhombohedral,[9] monoclinic,[13] and orthorhombic.[18] This latter structure, which can be considered as an intermediate structure between rhombohedral α-Fe_2O_3 and cubic γ-Fe_2O_3, appears to be the most probable.[20] Another source of controversy is the route by which ϵ-Fe_2O_3 forms; both γ-$Fe_2O_3 \rightarrow \epsilon$-$Fe_2O_3$ and β-FeO(OH) $\rightarrow \epsilon$-Fe_2O_3 have been suggested.[21−23] In unconfined samples, a wide range of temperatures, ~700 K[15] to ~1300 K,[9] have been reported for the transformation ϵ-$Fe_2O_3 \rightarrow \alpha$-$Fe_2O_3$; however, ϵ-Fe_2O_3 is reported to be stable up to ~1700 K when confined in the pores of a silica matrix.[17]

The magnetic properties of this material are far from being well understood. Ordered ϵ-Fe_2O_3 is ferrimagnetic with a Curie temperature of about $T_C = 490$ K,[12,13] but disordered ϵ-Fe_2O_3 has been reported to be antiferromagnetic with $T_N = 490$ K.[24] The material has been long known to exhibit rather large magnetic anisotropy.[24] Moreover, it has been recently shown that coercivities in excess of $H_C = 20$ kOe can be obtained in acicular ϵ-Fe_2O_3 nanoparticles;[4] the corresponding value for the widely used hexagonal magnetoplumbite $BaFe_{12}O_{19}$ is only $H_C = 7.5$ kOe, thus conferring to this material an important potential for technological applications. Consistent with the orthorhombic crystal structure, Mössbauer spectra[20] are interpreted as indicating four cation-sites: three octahedral and one tetrahedral.

We present a systematic optimization of the synthesis of ϵ-Fe_2O_3 in a silica matrix by sol−gel chemistry from tetraethoxysilane (TEOS) and iron nitrate precursors. Silica gel pores serve as nanovessels in which the transformation of iron-nitrate to ϵ-Fe_2O_3 phase takes place. Yields in excess of 93% ϵ-Fe_2O_3 and particle sizes up to 20 nm were achieved. Evidently, the supporting silica matrix stabilizes ϵ-Fe_2O_3 up to $T \approx 1600$ K, at which temperature ϵ-Fe_2O_3 starts to transform to α-Fe_2O_3. Our results confirm that ϵ-Fe_2O_3 is ferrimagnetic ($M_s \approx 25$ emu/g) with a large coercivity, $H_c \approx 20$ kOe, and $T_C \approx 510$ K.

2. Experimental Section

2.1. Synthesis. Sol−gel preparations followed a procedure similar to that described by Savii et al.[25] Iron nitrate (Riedel-de Haen, 96%) and tetraethoxysilane (TEOS) (Fluka, 98%) were used as precursors of the ϵ-silica nanocomposite. Targeted compositions ranged from 13 to 43 wt % Fe_2O_3. Hydrolysis and condensation processes occurred in acidic hydroethanolic medium at TEOS:H_2O:EtOH = 1:6:6 mole ratio, reaction pH ≈ 0.9. Reactions are self-catalyzed by the nitric acid, which results from the hydrolysis of iron nitrate. Gelation at room temperature took place after 20 days; wet gels were dried at 60−80 °C for 14 h. The dried xerogels were rather hard and had a red-brownish, translucent, glassy appearance. Samples were crushed in an agate mortar, and the resulting powders were subjected to thermal treatments between 300 and 1100 °C in air. This was done in air with 3 h of annealing every 100 °C, and then the samples were slowly cooled to room temperature. Samples are labeled as SX/T (where X represents the nominal weight percentage of Fe_2O_3 and T denotes the temperature of thermal treatment in °C).

2.2. Characterization. Elemental analysis of Fe and Si was performed with an inductively coupled plasma-mass spectroscopy (ICP-MS) system (Perkin-Elmer Optima 3200 RL) and by scanning electron microscopy with energy-dispersive X-ray analysis (EDX) in a JEOL JSM-6300 microscope equipped with an Oxford Instruments LINK ISIS-200 EDX.

Transmission electron microscopy (TEM) observations were carried out using a Philips CM 30 microscope operating at 300 kV and a Hitachi H800MT microscope operating at 200 kV. Before the TEM observations, the samples were crushed and ultrasonically dispersed in ethanol. Drops of the solution were subsequently deposited onto Cu TEM-grids that were coated with a conductive polymer, and the ethanol was allowed to evaporate. Particle size distributions were performed by sampling more than 150 particles from TEM micrographs and fitting data to log-normal distribution functions. Particle sizes are given as the diameter of the distribution maxima.

The formation of the crystalline phases was studied by X-ray diffraction (XRD) in a $\theta-2\theta$ Bragg−Brentano geometry using a Siemens D5005 powder diffractometer, with diffracted beam monochromator and Cu Kα radiation ($\lambda = 1.5406$ Å). Diffraction patterns were recorded from 10° to 90° with a step size of 0.1° and a scanning rate of 15 s per step. To quantitatively analyze the structural parameters, for example, phase percentages, crystallite sizes, or cell parameters, Rietveld refinements were performed using the MAUD program.[26] The orthorhombic (space group $Pna2_1$) structure, described by Tronc et al.,[20] and the usual trigonal structure (space group R-3c) were adopted for ϵ-Fe_2O_3 and α-Fe_2O_3, respectively. Modeling of the silica glass is based on the assumption that from the X-ray diffraction pattern it is not possible to distinguish if the structure is completely amorphous or nanocrystalline[27] SiO_2. This method approximates the SiO_2 amorphous phase as a nanocrystalline solid (cubic structure with space group $P2_13$) in which crystallite size is taken to be of the same order of magnitude as the cell parameters and the disorder is statistically introduced by the microstrain effect.[28]

(19) Note that because no Mössbauer spectroscopy studies were available in early studies such as in refs 9, 12, the purity of these materials is only assessed from X-ray diffraction. Due to the broad and overlapping peaks of this type of iron(III) oxide polymorphs, the phase percentage as obtained from XRD may have limited accuracy. Actually, in these systems, Mössbauer spectroscopy is perhaps the most accurate tool for phase quantification.

(20) Tronc, E.; Chanéac, C.; Jolivet, J. P. *J. Solid State Chem.* **1998**, *139*, 93.

(21) Zboril, R.; Mashlan, M.; Barcova, K.; Vujtek, K. *Hyperfine Interact.* **2002**, *139*, 597.

(22) Chanéac, C.; Tronc E.; Jolivet, J. P. *J. Mater. Chem.* **1994**, *6*, 1905.

(23) Ponce-Castañeda, S.; Martínez, J. R.; Palomares-Sánchez, S.; Ruiz, F.; Ayala-Valenzuela, O.; Matutes-Aquino, J. A. *J. Sol.-Gel Sci. Technol.* **2003**, *27*, 247.

(24) Dézsi, I.; Coey, J. M. D. *Phys. Status Solidi A* **1973**, *15*, 681.

(25) Savii, C.; Popovici, M.; Enache, C.; Subrt, J.; Niznansky, D.; Bakardzieva, S.; Caizer, C.; Hrianca, I. *Solid State Ionics* **2002**, *151*, 219.

(26) Lutterrotti, L.; Gialanella, S. *Acta Mater.* **1997**, *46*, 101.

(27) Le Bail, A. *J. Non-Cryst. Solids* **1995**, *183*, 32.

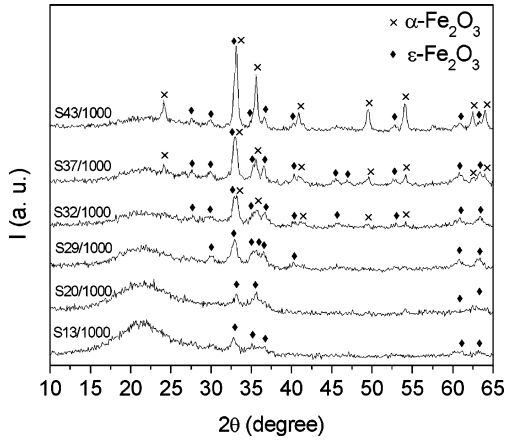

Figure 1. XRD patterns of the $SiO_2-\epsilon$-Fe_2O_3 composites of different compositions annealed at 1000 K.

Mössbauer spectra (MS) were acquired at room temperature (and for some samples at 80 and 4.2 K) using a conventional Mössbauer spectrometer with a ^{57}Co/Rh source for which velocity calibration was done using a 25 μm foil of metallic iron, and the Mössbauer parameters are given relative to this standard at room temperature.

Phase stability in the 300−1800 K range was studied by differential thermal analysis (DTA) on a Perkin-Elmer DTA 7 apparatus at several heating rates under an Ar atmosphere.

Magnetic thermogravimetry (MTG) measurements were performed in Ar atmosphere using a Perkin-Elmer TGA-7 instrument upon cooling at a 5 K/min rate from 1000 to 300 K, under an applied field of ∼25 Oe.

Hysteresis loops were measured at room temperature in fields up to 220 kOe using an extracting magnetometer at the Grenoble High Magnetic Fields Laboratory facility.

3. Results and Discussion

The ICP-MS elemental analysis for Fe and Si quantification performed on a sample of the S29 series was interpreted on the basis of SiO_2/Fe_2O_3 composite samples and revealed no deviations from the nominal composition (29 wt % Fe_2O_3), thereby excluding phenomena such as iron-precursor leaching during synthesis. This result was also confirmed, with reduced resolution, by performing quantitative elemental analyses on several samples by EDX spectroscopy. From these studies, the presence of less than a 5 wt % C and O in excess of the expected amount was established. The excess of oxygen probably originates from adsorbed water (also detected by DTA and MTG experiments) coordinated to hydroxyl groups. This conclusion is supported by ^{57}Fe Mössbauer studies, which detected only ferric iron.

Figure 1 is a set of XRD spectra corresponding to samples with different iron oxide contents, subjected to the same thermal treatment at 1000 °C. All of the patterns exhibit the characteristic silica glass hump centered around $2\theta = 22°$, plus several crystalline peaks. All peaks could be assigned to either α-Fe_2O_3 or ϵ-Fe_2O_3. As expected, an increase of relative intensity of the crystalline peaks with respect to the amorphous hump is observed as the sample iron content is raised. It is also apparent that ϵ-Fe_2O_3 is the major phase when the total iron oxide percentage is less than 37 wt %, but that α-Fe_2O_3 becomes the dominant phase in samples

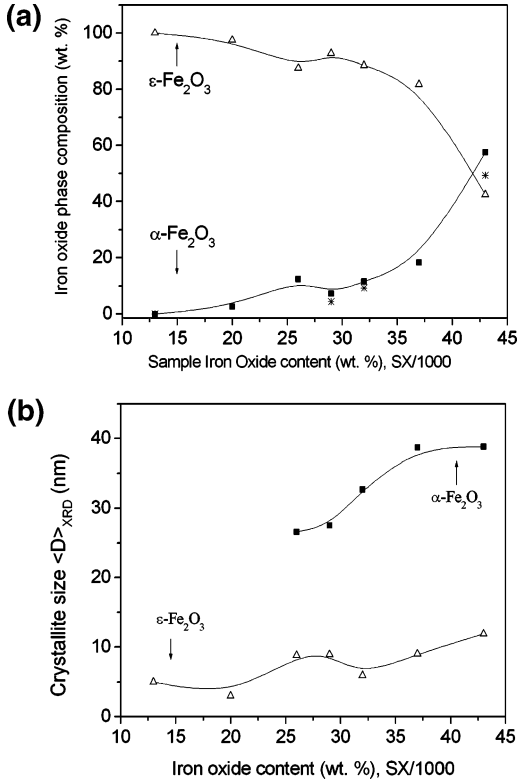

Figure 2. (a) Iron oxide phase composition as a function of the total iron oxide content. The α-Fe_2O_3 (■) and ϵ-Fe_2O_3 (△) weight compositions obtained from Rietveld analysis are presented together with α-Fe_2O_3 content given by Mössbauer measurements (∗). (b) Dependence of crystallite sizes for α-Fe_2O_3 (■) and ϵ-Fe_2O_3 (△) as obtained from Rietveld analysis on the total iron oxide content. The lines are guides to the eye.

with a total iron oxide content greater than 37 wt %. Figure 2a shows the phase percentages obtained from quantitative Rietveld fits. Up to about 30 wt % iron oxide content, the amount of ϵ-Fe_2O_3 remains above 93%, but a slight increase in α-Fe_2O_3 content is detected with increasing Fe content. This trend is drastically altered for iron oxide compositions exceeding 37 wt % in which hematite rapidly becomes the major polymorph.

Figure 2b displays the evolution of ϵ-Fe_2O_3 and α-Fe_2O_3 crystallite sizes versus the iron oxide concentration, as obtained from Rietveld refinement. Because amorphous SiO_2 is the major phase and the concentrations of the nanocrystalline phases (especially hematite) are low, there is a considerable uncertainty associated with the crystallite size determination. That said, the crystallite size, $\langle D \rangle$, is estimated as ∼10 nm for ϵ-Fe_2O_3 and ∼25−40 nm for α-Fe_2O_3. Both ϵ-Fe_2O_3 and α-Fe_2O_3 crystallite sizes are weakly dependent on the iron oxide concentration.

Mössbauer spectra of some of the samples in the SX/1000 series are shown in Figure 3. Spectra were fitted by assuming the presence of both ϵ-Fe_2O_3 (based on the parameters given by Tronc[20]) and α-Fe_2O_3. However, because two of the sites for ϵ-Fe_2O_3 have very similar parameters,[20] they have been fitted with only one single sextet. Therefore, the spectra were fitted to a total of three sextets with relative area ratios 1:1:2 corresponding to the four Fe-sites in ϵ-Fe_2O_3 plus an additional sextet for the Fe-site in α-Fe_2O_3. Table 1 shows the parameters that were used to fit the spectra for sample

(28) Lutterotti, L.; Ceccato, R.; Dal Maschio, R.; Pagani, E. *Mater. Sci. Forum* **1998**, *278−281*, 87.

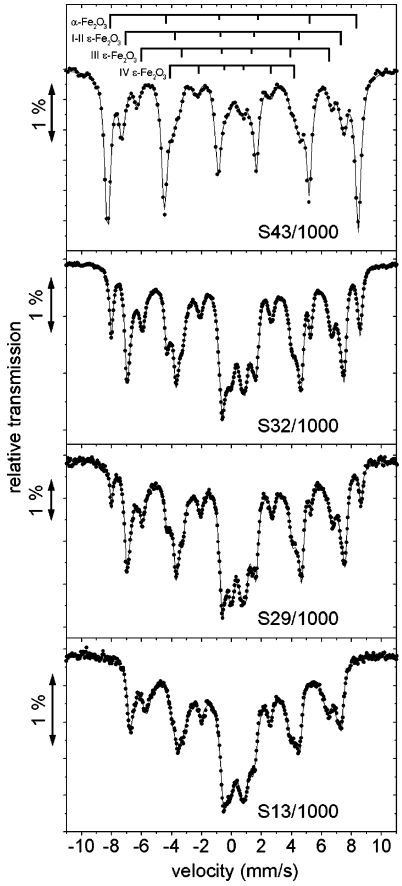

Figure 3. Room-temperature Mössbauer spectra from SiO_2−ϵ-Fe_2O_3 composites of different compositions annealed at 1000 K. At the top of the figure, the contributions of the different Fe sites are schematically presented. The continuous lines are fits to the parameters described in the text.

Table 1. Hyperfine Parameters Deduced from the 300 K Mössbauer Spectrum on Sample S29/1100[a]

		δ_{Fe} (mm/s) (±0.02)	2ϵ (mm/s) (±0.02)	Γ (mm/s) (±0.02)	B_{hf} (T) (±0.4)	*A* (%) (±2)
ϵ-Fe_2O_3	I−II	0.37	−0.27	0.45	44.5	40
	III	0.39	−0.04	0.47	38.7	25
	IV	0.23	−0.15	0.70	25.6	28
α-Fe_2O_3		0.39	−0.30	0.40	51.0	7

[a] δ_{Fe} is the isomer shift quoted relative to metallic Fe, 2ϵ is the quadrupolar shift, Γ is the fwhm of the band shift, all in mm/s, and B_{hf} is the hyperfine field in tesla. *A* is the percentage of the total resonant area associated with each subspectrum.

S29/1100. To fit most spectra, an additional doublet, for Fe magnetically unblocked superparamagnetic ϵ-Fe_2O_3 particles, was required. These particles are superparamagnetic because their magnetization-relaxation times are faster than the Mössbauer measurement time scale. The relaxation time is $\tau = \tau_0 \exp[KV/k_BT]$, where τ_0 is the time constant characteristic of the material, k_B is Boltzmans' constant, *K* is the magnetic anisotropy, *V* is the particle volume, and *T* is the temperature. These particles yield doublet spectra rather than a set of sextets.[29] This hypothesis was confirmed by low-temperature measurements in which the doublet component disappeared and the corresponding ϵ-Fe_2O_3 area subspectra increased, while the area of the hematite sextet remained constant (as shown later). Thus, hematite

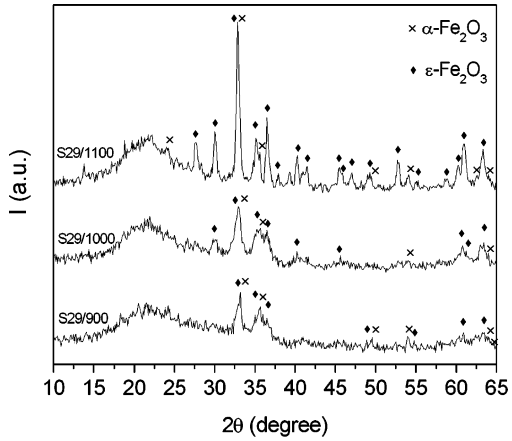

Figure 4. XRD patterns of the SiO_2−ϵ-Fe_2O_3 composites with 29 wt % Fe_2O_3 annealed at different temperatures.

particles are magnetically blocked at room temperature, which is consistent with the results of Bødker et al.[30] for crystallite sizes in the 25−40 nm range that are relevant to this study. The determination of the α-Fe_2O_3 relative concentration is readily obtained from the evaluation of the α-Fe_2O_3 sextet relative area, assuming that the recoilless fractions are the same for both polymorphs. Indeed, the increase of the most external hematite sextet observed in the room-temperature MS of Figure 3 is interpreted as an increase of the α-Fe_2O_3 content at higher iron oxide compositions. Note that for the smallest Fe content no α-Fe_2O_3 peak is observed, which suggests that pure ϵ-Fe_2O_3 was obtained. A plot of the phase percentages versus total iron oxide concentration, from both MS and XRD Rietveld refinement (Figure 2a), indicates good agreement between the two techniques.

The effect of the annealing temperature has been studied on the S29 series (29 wt % iron oxide) that has the highest Fe_2O_3/SiO_2 ratio with ϵ-$Fe_2O_3 \approx 93\%$. The XRD spectra obtained from some of these samples, annealed at different temperatures, are presented in Figure 4. A comparison of the different XRD patterns reveals that increasing the annealing temperature correlates with a sharpening of the ϵ-Fe_2O_3 diffraction peaks, which indicates that larger crystallite size is obtained by annealing at higher temperatures; for example, ϵ-Fe_2O_3 crystallite size ranges from $\langle D\rangle_{XRD} \approx$ 5 nm for S29/900 to $\langle D\rangle_{XRD} \approx$ 19 nm for S29/1100. Although the peak intensities increase with increasing annealing temperature, the area of the peaks, and thus the ϵ-Fe_2O_3 content, remain constant. The TEM image of sample S29/1100 (see Figure 5) shows the presence of roughly spherical nanosized particles, well isolated inside the silica matrix. The particle size obtained from the maximum of the log-normal distribution, 25 nm, is in good agreement with the XRD crystallite size for this sample. The same conclusion, that is, the correlation of larger crystallite size with higher annealing temperature, can be inferred from the RT Mössbauer spectroscopy results of this series (see Figure 6). The spectra reveal superparamagnetic behavior in the ϵ-phase which strongly depends on the annealing temperature and can be explained by differences in the volumes of the ϵ-Fe_2O_3 particles among these samples (see the equation for the

(29) Mørup, S. *Hyperfine Interact*. **1990**, *60*, 959.

(30) Bødker, F.; Mørup, S. *Europhys. Lett*. **2000**, *52*, 217.

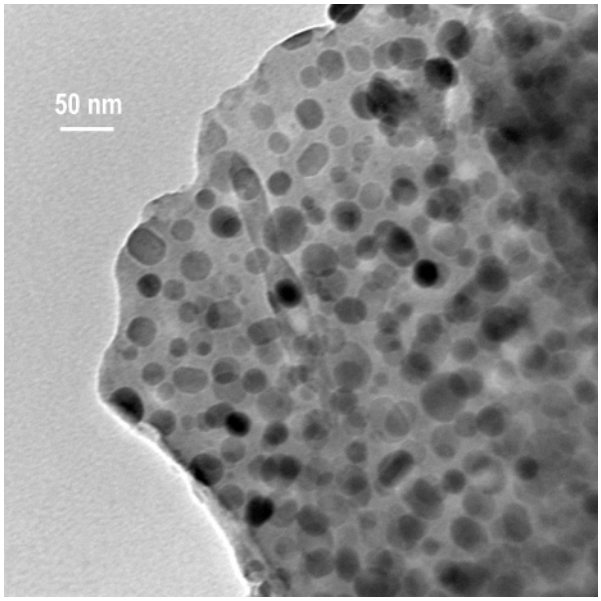

Figure 5. TEM image of the SiO_2–ϵ-Fe_2O_3 composite corresponding to sample S29/1100.

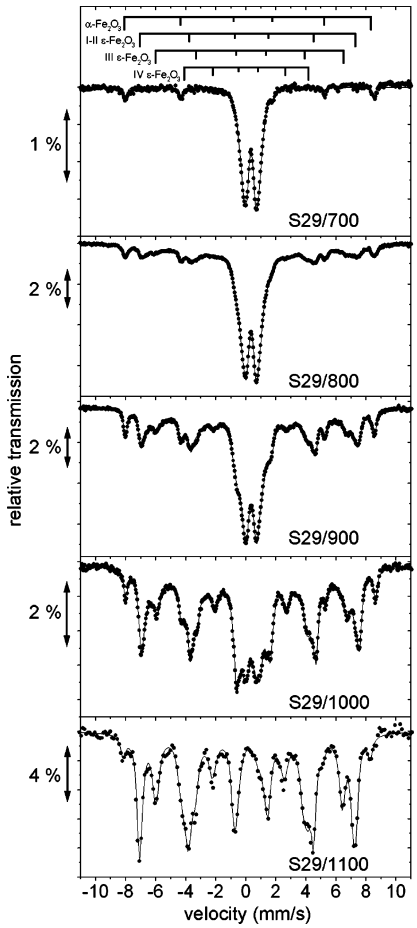

Figure 6. Room-temperature Mössbauer spectra from SiO_2–ϵ-Fe_2O_3 composites with 29 wt % Fe_2O_3 annealed at different temperatures. At the top of the figure, the contributions of the different Fe sites are schematically presented. The continuous lines are guides to the eye.

relaxation time of the magnetization). Note the different annealing temperatures seem to have no effect on α-Fe_2O_3 (most external sextet). However, the large doublet observed for sample S29/700 gradually transforms into the ϵ-Fe_2O_3 characteristic sextets as the

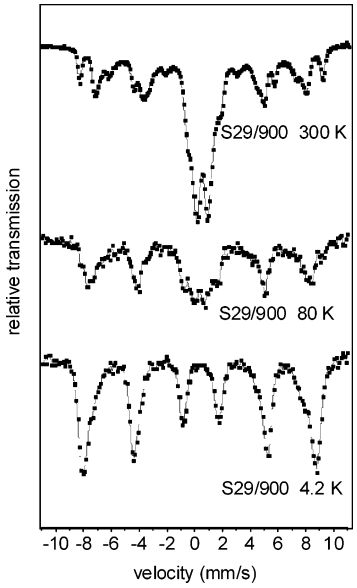

Figure 7. Temperature-dependent Mössbauer spectra corresponding to sample S29/900.

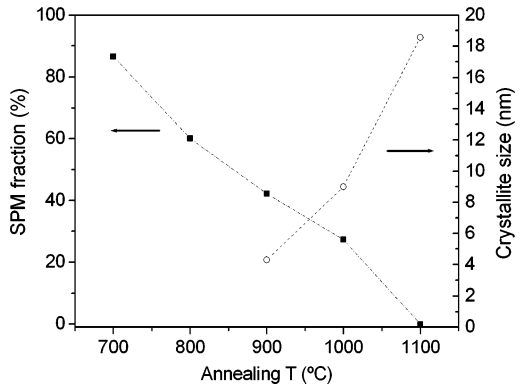

Figure 8. Influence of the annealing temperature influence on the ϵ-Fe_2O_3 crystallite size (△) and on the Mössbauer superparamagnetic fraction (■). The lines are guides to the eye.

samples are treated at progressively higher temperatures, completely disappearing for S29/1100. This implies that the relaxation time at room temperature, and consequently the particle size, becomes progressively larger for higher annealing temperatures. This is evidenced in Figure 7 where Mössbauer spectra at 4.2, 80, and 300 K for S29/900 are shown. A progressive increase of the blocked Mössbauer sextet subspectrum can be observed as the temperature is lowered. At 4.2 K, the spectrum is completely blocked. Even though for samples annealed at lower annealing temperature (700 and 800 °C) the blocking process is also observed by Mössbauer spectroscopy, the presence of some poorly crystalline iron oxide/oxyhydroxide phases precursors of the ϵ-phase cannot be excluded. However, most of such possible precursor phases are already not stable above 500 °C.[1] As expected, Figure 8 shows a good correlation between the increase of the ϵ-Fe_2O_3 XRD crystallite size and the decrease of the superparamagnetic fraction of the ϵ-Fe_2O_3 phase obtained from the MS fittings. Crystallite sizes in samples annealed at temperatures below 900 °C are not presented because the low crystallinity of these samples makes Rietveld refinements unreliable. Rietveld refinements also revealed no significant varia-

tion of the hematite phase percentage as a consequence of annealing in the 900−1100 °C range.

To investigate the thermal stability of ϵ-Fe_2O_3, DTA measurements of the S29/1000 sample were performed between room temperature and ∼1600−1800 K, at several heating rates. The DTA curves displayed no thermal process that could be assigned to the ϵ-Fe_2O_3 to α-Fe_2O_3 transformation. In fact, there are several reasons that could make the detection of the ϵ to α transformation by DTA in our samples difficult. On one hand, the content of ϵ-Fe_2O_3 never exceeds 30 wt % of the composite and the crucible capacity is limited to about 20 mg of sample. On the other hand, it is possible to assume that the transformation does not take place at a fixed temperature but rather in a range of temperatures. Indeed, XRD analysis of the sample after the DTA experiment revealed that the transformation had partially occurred: the pattern (not shown) of S29/1000 after being heated twice to ∼1600 K at 40 K/min presented the diffraction peaks corresponding both to α-Fe_2O_3 and to ϵ-Fe_2O_3 phases, and a comparison with the XRD spectrum of S29/1000 before the DTA runs revealed that the content of the former phase increased at the expense of the latter. This XRD spectrum also showed some transformation of the amorphous SiO_2 into the crystalline polymorph cristobalite. Moreover, the unexpectedly high intensity of the α-Fe_2O_3 (110) peak suggests the presence of Fe_3O_4, which has its most intense reflection, (311), located at the same 2θ value as α-Fe_2O_3 (110). To establish an upper limit for the thermal stability of ϵ-Fe_2O_3 and clarify which phases are stabilized at high temperature, a subsequent DTA analysis on S29/1000 sample was performed up to ∼1800 K. In this case, the run showed superimposed exothermal peaks starting at temperatures above 1600 K that after an XRD analysis of the heated sample were attributed to the transformation of amorphous silica into the cristobalite and tridymite-o crystalline polymorphs. This XRD spectrum revealed also no trace of ϵ-Fe_2O_3 and the presence of Fe_3O_4, which is the stable phase above 1700 K in an inert atmosphere.[31] Thus, we can conclude that for temperatures below 1600 K only a fraction of the ϵ-Fe_2O_3 nanoparticles embedded in amorphous SiO_2 transform to the more stable α-Fe_2O_3. At higher temperatures, when the silica crystallization takes place, the ferric oxides transform to Fe_3O_4. This behavior contrasts with the results obtained by Trautmann[12] et al. in a system containing nonconfined ϵ-Fe_2O_3 particles; they reported a transformation by DTA at ∼1000 K.

The formation and stability of ϵ-Fe_2O_3 can be qualitatively understood on the basis of the confinement imposed by the porous silica matrix. In principle, there is no general relation between the original iron precursor and the Fe_2O_3 crystalline structure obtained by thermal transformations.[2] Two factors determine both the formation of a given Fe_2O_3 phase from a precursor cluster and the transformations between polymorphs: the bulk free energies ΔG_V^i of the different i-Fe_2O_3 phases ($i = \alpha, \beta, \gamma, \epsilon$) and the energy barrier that must be overcome for the transformation to take place. Both factors depend on many parameters, and kinetics plays a key role in these processes. Actually, when the particle size is decreased to the nanometer range, the surface-to-volume ratio becomes more important and the surface energy σ_i has to be considered. The free energy variation per unit mass can be expressed as $\Delta G_m^i = (3\sigma_i/\rho_i r) - (\Delta G_V^i/\rho_i)$ for spherical crystallites of radius r of the ith polymorph, where ρ_i is the phase density.[32] Consequently, it can be inferred that even if $\Delta G_V^\alpha > \Delta G_V^\epsilon$, the metastable ϵ-Fe_2O_3 can be stabilized over α-Fe_2O_3 (i.e., $\Delta G_m^\epsilon < \Delta G_m^\alpha$), provided that $\sigma_\epsilon < \sigma_\alpha$ and the particle size is small enough. The latter condition can be imposed either by fast reaction kinetics or, as in the present case, by limiting the volume available for particle growth. The stabilization of metastable nanocrystalline polymorphs has been described in systems such as $BaTi_2O_3$, ZrO_2, or Al_2O_3[33−35] and in the case of iron oxide even an α-Fe_2O_3 to γ-Fe_2O_3 transformation by size reduction has been reported.[36] In our system, when Fe_2O_3 is formed by dehydroxylations of the FeO(OH) polymorphs, there is a replacement of hydroxy by oxo bonds and the structure is densified. This is followed by the development of microporosity due to expulsion of water and subsequent processes of micropore coalescence into macropores[2] that favor the diffusion and aggregation of the oxide particles. If particles grow large enough, the energy barrier impeding α-Fe_2O_3 formation is overcome and ϵ-Fe_2O_3 is no longer favored. The presence of the silica matrix prevents the process by limiting the growth of the forming nanoparticles to within the silica pores, thereby avoiding particle coalescence. The above expression for ΔG_m^i also allows a qualitative understanding of the increased thermal stability achieved with confinement in silica. Even if the temperature is high enough to supply the activation energy needed for the ϵ-Fe_2O_3 to α-Fe_2O_3 transformation, the nucleated hematite cannot be stabilized because the growth is still impeded due to the confinement; hence, any fluctuation will turn the α-Fe_2O_3 nuclei back to ϵ-Fe_2O_3. However, this no longer holds at temperatures above 1300 K due to the enhanced atomic diffusion. The fact that the pores in the SiO_2 matrix are actually interconnected can also explain why the α-Fe_2O_3 formation is favored above a "threshold" concentration of the Fe precursor: the increased iron nitrate volume fraction leaves less free space between the pores so that the distances between Fe_2O_3 growing clusters are smaller and diffusion between neighboring clusters at the temperatures of the oxide formation is permitted.

Figure 9 is a plot of two representative room-temperature hysteresis loops for the samples that contain ϵ-Fe_2O_3 nanoparticles. Sample S29/700 exhibits a hysteresis loop with zero remanence and zero coercivity typical of superparamagnetic samples, in agreement with the doublet observed in the Mössbauer spectrum of Figure 6. However, sample S29/1100 (with a completely blocked Mössbauer spectrum, as shown in Figure 6) exhibits a typical ferromagnetic (or ferrimagnetic)

(31) Darken, L. S.; Gurry, R. W. *J. Am. Chem. Soc.* **1946**, *68*, 798.
(32) Rana, S.; Ram, S. *Phys. Status Solidi A* **2001**, *201*, 427.
(33) Flaschen, S. S. *J. Am. Chem. Soc.* **1955**, *77*, 6194.
(34) Garvie, R. C. *J. Phys. Chem.* **1978**, *82*, 218.
(35) McHale, J. M.; Auroux, A.; Perrotta, A. J.; Navrotsky, A. *Nature* **1997**, *277*, 788.
(36) Randrianantoandro, N.; Mercier, A. M.; Hervieu, M.; Grenèche, J. M. *Mater. Lett.* **2001**, *47*, 150.

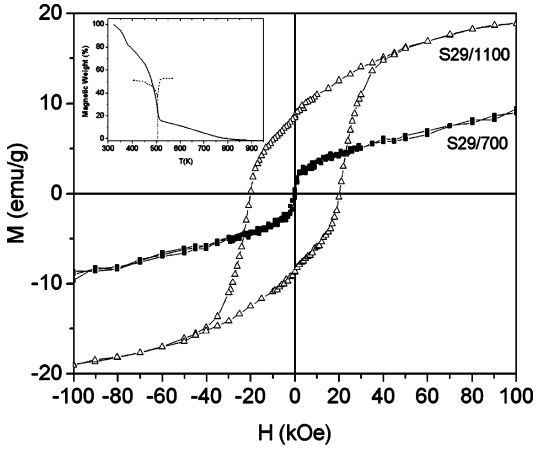

Figure 9. Room-temperature hysteresis loops of samples S29/700 (■) and S29/1100 (△). Shown in the inset is the MTG curve of sample S29/1000 and its derivative.

hysteresis loop with a coercivity of $H_C = 20$ kOe. These results are similar to what was reported for Ba-doped acicular ϵ-Fe_2O_3 nanoparticles which exhibited coercivites of up to $H_C = 20$ kOe.[4] The saturation magnetization of sample S29/1100 was estimated using the law of approach to saturation,[37] and a value $M_S \approx 13$ emu/g (mass of composite) was obtained. Taking into account the ϵ-Fe_2O_3 phase percentage, the saturation magnetization for the ϵ-Fe_2O_3 phase becomes $M_S = 25$ emu/g (mass of ϵ-Fe_2O_3), which is similar to the value reported by Jin et al. for Ba-doped ϵ-Fe_2O_3[4,38] and consistent with the values reported for isomorphic systems, such as $AlFeO_3$ or $FeGaO_3$.[39,40] The $M_S = 25$ emu/g value implies an average magnetic moment of $0.27\mu_B$ (Bohr magneton) per Fe ion. Because the expected moment for Fe^{3+} ions should be $5\mu_B$, this indicates that ϵ-Fe_2O_3 is ferrimagnetic, as proposed by Tronc et al. on the basis of Mössbauer measurements under applied fields.[20] Actually, the magnetic behavior of the studied samples correlates rather well with Mössbauer data. The samples exhibiting large doublets are superparamagnetic, while the ones showing clear sextets are ferrimagnetic with rather large coercivities. In addition, shown in the inset of Figure 9 is the MTG curve and its derivative for the S29/1000 sample. A sharp decrease in magnetic weight is evident at $T \approx 510$ K, which is consistent with the Curie temperature of ϵ-Fe_2O_3 reported by several authors.[12,13,24] The remanent magnetic force after this transition disappears around 900 K, similar to the Néel temperature of bulk α-Fe_2O_3 ($T_N = 956$ K[1]).

4. Conclusions

Sol−gel chemical synthesis of ϵ-Fe_2O_3 nanoparticles, embedded in a silica matrix, was investigated. Samples with ϵ-Fe_2O_3 phase percentages exceeding 93% were obtained with Fe_2O_3/SiO_2 ratios up to 30% and heat treatments above $T = 700$ °C. Transmission electron microscopy observations reveal that ϵ-Fe_2O_3 particles optimized for maximum content are roughly spherical and have sizes of around 25 nm. The magnetic properties of the samples range from superparamagnetism to a ferrimagnetic behavior with a Curie temperature of 510 K and a coercivity of 20 kOe at room temperature, depending on the synthesis conditions. Interestingly, it is found that this phase remains stable up to very high temperatures, that is, $T \approx 1600$ K. The fact that the nanoparticles are confined inside the pores of a xerogel plays an important role in the formation and enhanced thermal stability of this phase, evidencing the interest of exploring chemical transformation in spatially restricted fields.

Acknowledgment. Partial support from project 6/2001 of NATO program of the Czech Republic, Generalitat de Catalunya (Grant 2001SGR00335 and 2001SGR00189), Ministerio de Educación y Ciencia (Grant MAT-2003-01052 and MAT-2004-01679), and the EU Human Potential Program (Grant HPMT-CT2000-0006 and HPRI-1999-CT00030) is acknowledged. We are grateful to J. Oró and Dr. A. Fuertes for their assistance in thermal analysis measurements and to Dr. B. P. Burton for the critical reading of the manuscript.

CM048628M

(37) Chikazumi, S. *Physics of Magnetism*; John Wiley & Sons: London, 1978.
(38) Note that in ref 4 the value of magnetization, M, at 70 kOe is given rather than the saturation magnetization, M_S.
(39) Schieber, M.; Frankel, R. B.; Blum, N. A.; Foner, S. *J. Appl. Phys.* **1967**, *38*, 1282.
(40) Abrahams, S. C.; Reddy, J. M. *Phys. Rev. Lett.* **1964**, *13*, 688.